Clinical Biomechanics 24 (2009) 708–715

Contents lists available at ScienceDirect

Clinical Biomechanics

journal homepage: www.elsevier.com/locate/clinbiomech

The effect of landmarks and bone motion on posture-related changes in carpal tunnel volume

Jeremy P.M. Mogk [a], Peter J. Keir [b,*]

[a] Sensory Motor Performance Program, Rehabilitation Institute of Chicago, Chicago, IL, USA
[b] Department of Kinesiology, McMaster University, 1280 Main Street West, Hamilton, ON, Canada L8S 4K1

ARTICLE INFO

Article history:
Received 10 October 2008
Accepted 7 May 2009

Keywords:
Carpal tunnel syndrome
MRI
Volume
Wrist
Three-dimensional reconstruction
Modelling

ABSTRACT

Background: Deviated wrist postures have been linked to carpal tunnel syndrome development, yet the effect of posture on carpal tunnel volume remains unclear. The purposes of this study were (i) to evaluate the effect of boundary definitions on tunnel volume estimates in neutral and non-neutral (30° flexion, 30° extension) wrist postures and (ii) to develop a biomechanical wrist simulation to predict posture-related changes in tunnel volume.
Methods: Two carpal tunnel volume measures were calculated using (i) ulnar bony landmarks and (ii) radial and ulnar bony landmarks identified directly from magnetic resonance imaging (MRI) scans. A third volume measure combined computerized tunnel reconstructions with modelled bone surfaces to calculate an anatomically landmarked volume. Six individual simulations were then generated to predict volume in the flexed and extended postures based on individual carpal bone motions.
Findings: Boundary definitions influenced the absolute volume in each posture and the relative changes between postures. Relative to fully reconstructed volumes, radial and ulnar landmarked volumes were 15–25% larger across postures (681 (SD 467) mm^3; $P = 0.01$), while the ulnar-only landmarked volumes were 10–20% smaller (562 (343) mm^3; $P < 0.01$). Simulation predicted volumes were not significantly different from the reconstructed anatomically landmarked volumes, with less inter-individual variability between postures compared to MRI-based volumes.
Interpretation: Comparison of volume measures indicated the importance of capturing posture-related changes in the orientation of the proximal and distal tunnel boundaries, and revealed potential sources of error associated with volume reconstruction. Simulations can enable changes in tunnel dimensions to be related to bone movements throughout a range of motion.

1. Introduction

Deviated wrist posture has been identified as a risk factor for carpal tunnel syndrome (CTS) in the workplace, particularly when combined with forceful and/or repetitive hand tasks (Armstrong and Chaffin, 1979; Silverstein et al., 1987). Non-neutral postures have been suggested to compress the median nerve within the carpal tunnel, as evidenced by increased hydrostatic pressure and mechanical impingement (generally with wrist extension and flexion, respectively) (Smith et al., 1977; Gelberman et al., 1981; Keir et al., 1997; Keir et al., 1998; Luchetti et al., 1998; Rojviroj et al., 1990; Weiss et al., 1995). Carpal tunnel pressure varies with wrist posture and is thought to reflect absolute or relative changes in carpal tunnel volume (CTV) (Robbins, 1963; Skie et al., 1990; Yoshioka et al., 1993; Bower et al., 2006), although the latter has yet to be demonstrated empirically. Detailed image-based modelling of the carpal tunnel is needed to delineate the relationship between posture-related changes in tunnel shape, volume and pressure.

Anatomically, the carpal tunnel is traditionally defined as the fibro-osseous tunnel on the palmar side of the wrist formed by the concave arch of the carpal bones and enclosed palmarly by the transverse carpal ligament (TCL) (Robbins, 1963; Sora and Genser-Strobl, 2005). The TCL attaches ulnarly to the pisiform and hook of the hamate, and radially to the scaphoid tubercle and ridge of the trapezium, and is sometimes synonymously called the flexor retinaculum (FR) (Middleton et al., 1987; Mesgarzadeh et al., 1989; Nigro, 2001). However, a detailed examination of cadaveric specimens revealed that the FR extends from the distal radius to the distal aspect of the base of the third metacarpal, with the TCL representing the central portion of the FR which "serves as the roof of the *anatomic* carpal tunnel" (Cobb et al., 1993). Consequently, Cobb et al. (1993) suggested that the palmar boundary of the carpal tunnel be redefined to include the fascial extensions proximal and distal to the TCL. Nonetheless, the bony landmarks used to define CTV boundaries are variable. Proximal boundary definitions have included the radiocarpal joint (Pierre-Jerome et al.,

* Corresponding author. Department of Kinesiology, McMaster University, 1280 Main Street West, Hamilton, ON, Canada L8S 4K1.
E-mail address: pjkeir@mcmaster.ca (P.J. Keir).

0268-0033/$ - see front matter © 2009 Published by Elsevier Ltd.
doi:10.1016/j.clinbiomech.2009.05.012

1997a,b,c), the distal tip of the radial styloid (Cobb et al., 1992), the most proximal aspect of the pisiform (Bower et al., 2006), and the distal edge of the scaphoid (Richman et al., 1987, 1989; Ablove et al., 1994). Distal boundary definitions include the distal aspect of the hook of the hamate (Cobb et al., 1992; Bower et al., 2006), the bases of the metacarpals (Ablove et al., 1994; Pierre-Jerome et al., 1997a,b,c), and the appearance of the flexor pollicis longus tendon diverging from the other flexor tendons (Richman et al., 1987, 1989). Based on common measurement locations of carpal tunnel dimensions and pressure reported in the literature, the focus of this communication was placed on the volume defined by the four bony attachments of the TCL.

Measures of carpal tunnel size, such as cross-sectional area (CSA), have been determined using magnetic resonance imaging (MRI) (Cobb et al., 1992; Pierre-Jerome et al., 1997a,b,c; Bower et al., 2006). Carpal tunnel dimensions are typically reported at specific bony landmarks, such as the pisiform and hook of the hamate, and change with wrist flexion and extension (Skie et al., 1990; Yoshioka et al., 1993; Horch et al., 1997; Bower et al., 2006), likely due to carpal bone and thus carpal tunnel boundary movement with wrist motion (*c.f.* Kobayashi et al., 1997). Furthermore, efforts to determine CTV have been limited to the neutral wrist (Richman et al., 1987, 1989; Cobb et al., 1992; Pierre-Jerome et al., 1997a,b,c), with non-neutral wrist postures examined only recently (Bower et al., 2006). Carpal tunnel volume is typically calculated via integration of areas from sequential digitized slices, making volume dependent on slice thickness and the number of slices between proximal and distal landmarks (related to hand/wrist size). Thinner slices may allow more consistent landmark recognition, yet signal strength may be inadequate to identify all structures. Due to the axial progression of images, previous studies have assumed (i) that the radial and ulnar aspects of the tunnel are equal in length and (ii) that the proximal and distal boundaries are parallel, neither of which may be true (Bower et al., 2006). Given that posture-related changes in tunnel volume and shape are partially contingent on individual bone motions, it is essential to consider the positions of all four bony attachments of the TCL. Linking changes in carpal tunnel shape to the wrist bones would enable potential errors associated with volume rendering from MRI to be assessed.

Three-dimensional visualization improves traditional two-dimensional methods by enabling observation and measurement from multiple perspectives, and would facilitate evaluation of previously unavailable measures (Fig. 1, right-hand column). Computer reconstruction has been used previously to examine dimensions throughout the carpal tunnel length (Pierre-Jerome et al., 1997a,b,c); however, CSAs were depicted as circular discs aligned by the centre point which created a simplified structure limited to the neutral wrist. More recently, reconstruction of the carpal tunnel in neutral, flexed and extended wrist postures was performed without reshaping each digitized area (Mogk and Keir, 2007; Mogk and Keir, 2008). The process demonstrated the effects of image orientation on apparent size and shape of the carpal tunnel (Mogk and Keir, 2008), and indicated the need to evaluate posture-related changes in tunnel boundaries (Mogk and Keir, 2007). By reconstructing bony elements from MRI and incorporating them

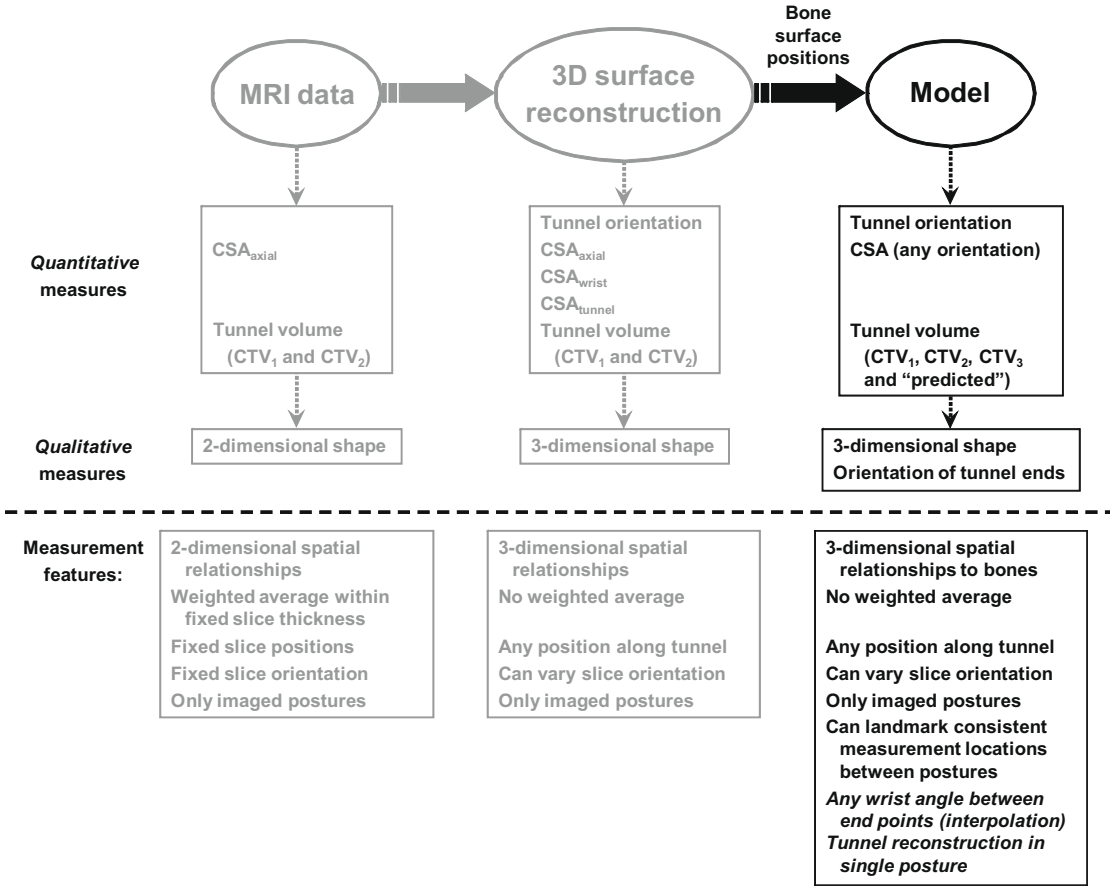

Fig. 1. The process used to construct and validate the individually scaled models of the wrist and carpal tunnel. Measures used for comparison are aligned horizontally above the dotted line, with measurement features provided by each data source compared in boxes below the dotted line. Italicized points in the right-hand column pertain to simulations using bone motions to predict posture-related changes in carpal tunnel size and shape. Previous evaluation of three-dimensional reconstruction is included in grey to illustrate the progression (adapted from Mogk and Keir, 2007).

into wrist-specific simulations, changes in the carpal tunnel can be linked to bone movement and may better represent CTV as a function of wrist posture.

The purposes of this study were (i) to evaluate carpal tunnel volume in neutral and deviated wrist postures using several boundary definitions and (ii) to develop a wrist simulation to predict posture-related changes in carpal tunnel volume based on carpal bone motions. While landmark selection will alter volume measurements, we hypothesized that landmark identification using three-dimensional reconstructions of the wrist and carpal tunnel would improve the consistency of the relative changes in CTV between postures compared with the two-dimensional methods. Ultimately, the goal of this simulation is to model carpal tunnel pressure and median nerve impingement.

2. Methods

Contours of the bones and carpal tunnel were digitized from existing MRI data of three splinted wrist postures (30° flexion, neutral and 30° extension) (Bower et al., 2006), and imported into the Maya™ software package (v7.0, Alias®, Toronto, Canada). Of eight existing image datasets, only six (4 male and 2 female) had sufficient axial range to be modelled. The bones (radius, ulna, eight carpal bones and five metacarpals) and carpal tunnel were manually traced from the distal radius to the metacarpal bases, consisting of 14–24 (3 mm contiguous) slices for each posture, depending on hand size. The dorsal and palmar carpal tunnel borders were defined as the inner surface of the palmar and transverse carpal ligaments, respectively. The right (dominant) wrist was imaged in each case, using a 1.5 T imaging system (General Electric, Milwaukee, WI, USA), with the hand positioned in an index finger pulp pinch posture. Wrists were splinted in each posture with no noticeable radial–ulnar deviation. Individuals had a mean age of 26.8 (SD 2.1) years, wrist circumference of 16.3 (1.4) cm and wrist width of 6.5 (0.6) cm. All volunteers were from the University community, self-identified as healthy and non-symptomatic at the time of testing, and reported no history of hand, wrist or forearm dysfunction.

2.1. Construction and development of individual wrist models

A set of 15 three-dimensional bone surfaces was imported from a public domain (http://www.3dcadbrowser.com), and an individual scaling factor was determined for each wrist based on capitate bone dimensions. The capitate bone was selected to establish scaling factors since the capitate appeared in the greatest number of MRI slices for each individual, as well as in each imaged posture. The imported capitate bone surface was uniformly scaled (along all three axes) and, using multiple views, was visually aligned to fit as closely as possible within the boundaries of the digitized capitate contours from the neutral wrist posture. This scaling factor was applied to all other bone surfaces, based on recent evidence that each carpal bone scales homogeneously as a function of wrist size (Crisco et al., 2005). The radius and ulna were fixed, with the radius used as a common reference to align all digitized contours from the three imaged postures.

2.1.1. Carpal tunnel surfaces

A non-uniform rational B-spline function (a form of Bézier spline) was used to reconstruct the carpal tunnel surfaces from the digitized x–y coordinates in the neutral wrist posture. Reconstructed contours were divided into two curves using break points at the TCL bony attachments on each side of the carpal arch to create two functional carpal tunnel surfaces; one representing the ligaments of the bony carpal arch, and the other representing the TCL.

2.1.2. Wrist (carpal bone) motion

For each wrist model, individually scaled bone surfaces were visually positioned according to the digitized MRI contours. After positioning all bone surfaces in the neutral posture, bone locations and orientations were recorded, and the procedure was repeated for 30° overall wrist flexion and 30° extension. Bone positions and orientations between these three postures were linearly interpolated to approximate bone motion between the three set positions. Early in the model development, carpal kinematics from the literature were used to confirm accurate prediction of bone motions, comparing interpolated bone locations (between end points) with those measured experimentally in 5° increments of flexion-extension (Moojen et al., 2002).

Three-dimensional translations and rotations of the individual carpal bones were used to drive changes in the carpal tunnel surfaces from the neutral posture. Carpal tunnel deformation, relative to the neutral posture, was the weighted result of bone motions on each carpal tunnel surface vertex. Tunnel surface vertices were "bound" to bone surface vertices, such that the influence of each bone on a given tunnel surface vertex varied according to the size and proximity of the bone. Changes in the dorsal tunnel surface (carpal arch) were based on all eight carpal bones, while the palmar surface (TCL) changed with only the four bony attachments (scaphoid and pisiform proximally, and trapezium and hamate distally).

2.2. Carpal tunnel volume calculation

Three CTV calculations were used to evaluate the effect of boundary definitions on CTV measured in each wrist posture. The first two measures, termed "CTV_1" and "CTV_2", used bony landmarks identified directly from MR images to define proximal and distal carpal tunnel boundaries, as has been done traditionally. CTV_1 used ulnar bony landmarks only (pisiform and hamate), while CTV_2 included radial bony landmarks as well (scaphoid and trapezium). These two MRI-based volumes represented mathematical reconstructions, which reflected the constraints of imaging and thus assumed that (i) the tunnel ends remained parallel regardless of wrist posture and (ii) the radial and ulnar aspects of the tunnel were equal in length (Fig. 2a and b). The third measure, "CTV_3", defined the carpal tunnel anatomically using the same four bony landmarks as CTV_2 without the constraint of parallel ends and allowing radial and ulnar aspects of different lengths (Fig. 2). CTV_3 was defined according to the TCL attachment sites described by Cobb et al. (1993), who asserted that the TCL forms the palmar boundary of the "*anatomic* carpal tunnel". This landmarked volume represented a static model which combined computerized tunnel reconstructions (from MRI) with modelled bone surfaces, using the bone surfaces to identify the carpal tunnel boundaries. The ends of the tunnel were assumed to be perpendicular to the dorsal tunnel surface in each posture (Fig. 2e). Individual wrist simulations were evaluated using a "predicted" volume measure, which was calculated from each simulation using the same definitions as CTV_3, but predicted volumes in flexion and extension based on the motion of the carpal bones. Predicted volumes were the result of the dorsal and palmar carpal tunnel surface deformations which occurred as a function of the individual carpal bone motions, relative to the neutral posture. Definitions for each volume measure are outlined in Table 1.

2.3. Statistics

Repeated measures ANOVAs were performed to evaluate the effects of wrist posture on the absolute carpal tunnel volume measures (STATISTICA, v6.0, StatSoft, Inc., Tulsa, OK). Significance was set at $P = 0.05$ with further evaluations using contrast analyses.

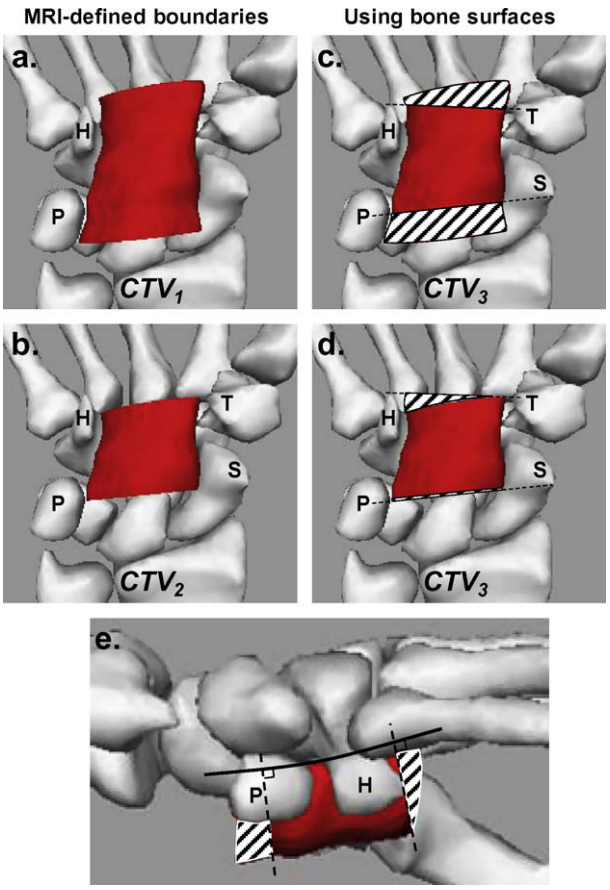

Fig. 2. Schematic comparison of volume measures, illustrating proximal and distal tunnel boundaries relative to the bony landmarks used to define them (P = pisiform, S = scaphoid, H = hamate, T = trapezium), in the neutral posture. (a) CTV_1 and (b) CTV_2 boundary definitions, using 2 and 4 bony landmarks, respectively, as identified directly from MRI. (c–e) Landmarked volume (CTV_3), using the modelled bone surfaces to identify specific bony landmarks to define proximal and distal boundaries (dotted lines). Cross-hatched areas outside of the landmarked volume indicate extra and missing volume based on CTV_1 (c and e) and CTV_2 (d) criteria, respectively. Bone surfaces were included in (a) and (b) to allow visual comparison of the MRI-based volume definitions with that of the landmarked method of the static models.

Unless an *F*-statistic is presented, *P*-values reflect those determined using planned contrasts.

3. Results

The carpal tunnel volumes measured using each boundary definition are summarized in Table 2. A significant interaction was found between boundary definition and wrist posture ($F_{4,20}$ = 5.62, $P < 0.01$). Specifically, CTV_1 decreased from neutral to non-neutral postures, with a mean reduction of 0.9% in flexion and 8.6% in extension (Table 2). CTV_2 decreased 11.3% from neutral to flexion, but increased 2.2% with extension (Table 2). CTV_3 decreased significantly from neutral to both wrist flexion (6.9%; $P < 0.001$) and extension (8.1%; $P < 0.001$). Examination of the boundary definition main effect ($F_{2,10}$ = 30.23, $P < 0.001$) revealed that CTV_1 measures were always larger than CTV_3 ($P = 0.01$), which were larger than CTV_2 ($P < 0.01$). The CTV_1 criteria resulted in volumes an average of 18.3% (SD 11.6%) larger than the anatomical landmarked measure (CTV_3) across postures (16.4% in neutral; 23.4% in flexion; 15.1% in extension). Conversely, the CTV_2 criteria resulted in volumes an average of 16.0% (8.9%) smaller than CTV_3 across postures (17.8% in neutral; 21.6% in flexion; 8.6% in extension).

Individual simulations were evaluated by comparing predicted CTV with the CTV_3 values measured in extension and flexion. Qualitative examination indicated that predicted changes to the dorsal surface (bony carpal arch) closely matched the tunnel reconstructions for each wrist; however, the predicted palmar surface (TCL) behaviour did not fully capture the extent of ligament surface tightening observed in extension or bowing in flexion (Fig. 3). Simulations predicted changes in the orientation of the tunnel ends similar to those seen with CTV_3 for each static model. Quantitatively, predicted volumes in flexion and extension were not statistically different from landmarked volumes, with reductions of 6.4% (1.2%) from neutral to 30° flexion ($P < 0.001$) and 7.0% (2.1%) for 30° extension ($P < 0.01$; Table 2). Cross-sectional areas throughout the predicted volumes, though not statistically different from reconstructed tunnels, were an average of 1.0% (8.1%) larger in extension and 3.1% (5.9%) smaller in flexion.

4. Discussion

In this study, carpal tunnel volume (CTV) was evaluated in neutral and non-neutral wrist postures by changing carpal tunnel boundary definitions (based on bony landmark identification) using reconstruction and modelling techniques. Individual three-dimensional biomechanical simulations were created for six wrists to predict posture-related changes in CTV through a 60° range of wrist flexion-extension, based on individual-specific carpal bone positions and orientations. Incorporation of completed bone surfaces enabled specific bony prominences to be consistently located in each posture, and between individuals, which contributed to the reduced CTV variability in the static models compared to mathematical volume reconstructions from MRI scans. The described simulations were the first to implement carpal bone motions to predict changes in carpal tunnel size, shape and orientation.

Table 1
Definitions of carpal tunnel volume (CTV) measures.

Volume measure	Definition
Reconstructed tunnel surfaces:	
(i) CTV_1	– MRI-based calculation, using slices from the most proximal aspect of the pisiform to the most distal aspect of the hamate – Only ulnar bony landmarks identified to define proximal and distal tunnel boundaries
(ii) CTV_2	– MRI-based calculation, from the most proximal slice containing both the pisiform and scaphoid tubercle to the most distal slice with the hook of the hamate and the ridge of the trapezium – Radial and ulnar bony landmarks used to define proximal and distal tunnel boundaries
(iii) CTV_3	– Static model, using tunnel reconstructions with bone surfaces to define the proximal border as a line bisecting the pisiform and the scaphoid tubercle, while the distal border ran between the most distal aspects of the hook of the hamate and trapezial ridge – The location identified on each bone corresponded to a specific vertex on the modelled bone surface – Represents bony attachments of the transverse carpal ligament, which is the central portion of the flexor retinaculum (Cobb et al., 1993)
Individual simulations:	
(iv) "Predicted"	– Same landmarks as defined for CTV_3, with interpolated carpal bone motions driving changes in carpal tunnel volume (relative to neutral) with wrist flexion and extension

Table 2
Calculated volume measures (mm^3) in neutral and non-neutral wrist postures, for each male (M) and female (F). MRI-based volumes were more variable between individuals than landmarked and predicted measures, showing both increases (italics) and decreases (plain text) in tunnel volume from neutral. Neutral posture landmarked volume was the starting point for each model. Relative changes in volume from the neutral posture are in parentheses. Significant differences at $P < 0.01$ are indicated by letters. Capital letters represent posture contrasts (across columns): A = extension vs. neutral; B = extension vs. flexion; C = neutral vs. flexion. Lower case letters represent contrasts between volume measures (across rows): $a = CTV_1$ vs. CTV_2; $b = CTV_1$ vs. CTV_3; $c = CTV_2$ vs. CTV_3.

Volume measure	Wrist #	Wrist posture		
		30° Extension	Neutral	30° Flexion
CTV_1	M1	4858.7 (−10.2%)	5411.3	*5441.0 (0.5%)*
	M2	3915.8 (−23.5%)	5118.3	4363.0 (−14.8%)
	M3	*4621.4 (7.6%)*	4295.8	*4906.8 (14.2%)*
	M4	4221.6 (−10.6%)	4723.6	4671.7 (−1.1%)
	F1	3652.0 (−10.6%)	4082.8	4080.6 (−0.1%)
	F2	2261.7 (−4.1%)	2358.7	2252.3 (−4.5%)
	Mean	**3921.9 (−8.6%)**	**4331.8**	**4285.9 (−0.9%)**
	SD	925.8 (10.1%)	1085.7	1100.2 (9.3%)
	Significance	B, a,b	a,b	B, a,b
CTV_2	M1	*3565.4 (4.1%)*	3426.3	3412.8 (−0.4%)
	M2	*3310.7 (2.6%)*	3226.5	3096.9 (−4.0%)
	M3	*3154.8 (1.7%)*	3101.1	2435.9 (−21.5%)
	M4	*3714.7 (4.0%)*	3573.0	2977.9 (−16.7%)
	F1	*3061.7 (4.2%)*	2938.5	2368.4 (−19.4%)
	F2	1829.4 (−3.4%)	1894.0	1785.8 (−5.7%)
	Mean	**3106.1 (2.2%)**	**3026.6**	**2679.6 (−11.3%)**
	SD	671.9 (2.9%)	599.1	592.6 (9.0%)
	Significance	B, a, c	C, a, c	B, C, a, c
CTV_3	M1	3824.1 (−10.0%)	4247.5	3869.6 (−8.9%)
	M2	3624.1 (−8.6%)	3964.1	3701.3 (−6.6%)
	M3	3629.2 (−7.3%)	3915.0	3672.2 (−6.2%)
	M4	3596.4 (−6.3%)	3838.7	3640.2 (−5.2%)
	F1	3537.1 (−7.9%)	3841.7	3541.7 (−7.8%)
	F2	2097.8 (−8.7%)	2297.2	2144.6 (−6.6%)
	Mean	**3384.8 (−8.1%)**	**3684.0**	**3428.3 (−6.9%)**
	SD	637.9 (1.3%)	695.9	637.9 (1.3%)
	Significance	A, B, b, c	A, C, b, c	B, C, b,c
Predicted	M1	3931.3 (−7.4%)	4247.5	3941.2 (−7.2%)
	M2	3746.3 (−5.5%)	3964.1	3756.1 (−5.2%)
	M3	3536.2 (−9.7%)	3915.0	3630.1 (−7.3%)
	M4	3651.1 (−4.9%)	3838.7	3631.0 (−5.4%)
	F1	3490.5 (−9.1%)	3841.7	3539.7 (−7.9%)
	F2	2178.8 (−5.2%)	2297.2	2173.4 (−5.4%)
	Mean	**3422.4 (−7.0%)**	**3684.0**	**3445.3 (−6.4%)**
	SD	629.3 (2.1%)	695.9	638.4 (1.2%)
	Significance	A	A, C	C

The carpal tunnel simulations coupled carpal tunnel surface motions with modelled bone motions to allow prediction of posture-related changes in carpal tunnel size, shape and orientation (including the tunnel ends) in absolute terms and relative to the neutral posture. Predicted volumes in flexion and extension were not statistically different from the anatomically landmarked CTV_3 values, thus indicating reproduction of posture-related changes in carpal tunnel shape using carpal bone motion. While the CSA measures throughout each tunnel were well predicted, subtle qualitative differences were noted with the TCL surface, specifically the lack of tightening in extension and bowing with flexion observed in the MRI reconstructions (Fig. 3). In the current simulations, TCL surface deformation was solely influenced by carpal bone motion. However, qualitative comparison of the palmar surface shape (Fig. 3) supports the future inclusion of TCL material properties to improve anatomic fidelity. Further incorporation of musculotendinous units would allow investigation of muscle loading conditions, which transmit forces to the TCL via the finger flexor tendons within the tunnel as well as other tendons attached to the external TCL surface (Keir et al., 1997; Kung et al., 2005). Inclusion of the structures passing through the carpal tunnel is further supported by recent finite element modeling of the effects of contact forces and fluid pressure on median nerve compression (Ko and Brown, 2007). The individual simulations provided continuity between imaged postures to allow examination of any wrist angle between 30° flexion and 30° extension, an improvement over the static models used to calculate landmarked volume. This feature could be used to identify the posture where the largest volume occurs, while extrapolation to more deviated wrist postures would expand the modelled range of motion. While not empirically evaluated in the current study, the model could also be used to examine the influence of atypical bone motions on tunnel dynamics, which could result from ligament injury (*c.f.* Werner et al., 2005). Furthermore, simulations require tunnel reconstruction only for a single posture, and then use posture-specific carpal bone positions and orientations to predict changes in tunnel volume within a given range of motion.

The three carpal tunnel boundary definitions examined resulted in significant differences in absolute tunnel volume for each posture, and relative volume changes between postures. MRI-based boundary definitions consisted of the commonly identified bony landmarks used to compare proximal and distal carpal tunnel size in the literature. On average, the CTV_1 method of identifying only ulnar bony landmarks from MRI produced volumes 681 mm^3 (SD 467 mm^3) larger than the anatomically landmarked CTV_3 measure, while the radial–ulnar landmark criteria of CTV_2 were 562 mm^3 (343 mm^3) smaller. Consequently, relative to landmarked volume, CTV_1 criteria yielded 15–25% larger volumes across postures, whereas the CTV_2 definition resulted in 10–20% smaller volumes, with the largest mean errors in flexion. Although only one study has calculated CTV in neutral and non-neutral postures (Bower et al., 2006), the current findings are pertinent in light of the number of CSA studies that have used bony landmark criteria similar to CTV_1 (Yoshioka et al., 1993; Bower et al., 2006) and CTV_2 methods (Dekel et al., 1980; Merhar et al., 1986;Horch et al., 1997; Monagle et al., 1999; Uchiyama et al., 2005). A detailed examination of the effects of wrist posture on carpal tunnel size and shape, including CSA, are detailed in a companion paper (Mogk and Keir, 2008). While a gold standard for carpal tunnel volume has yet to be established, the current investigation demonstrated the advantage of combining bone surface models with three-dimensional tunnel reconstruction to identify carpal tunnel boundaries, rather than sole reliance on two-dimensional images and numerical integration. This combined method for volume estimation may facilitate future examination of the relationship between carpal tunnel volume and pressure, and help to establish a gold standard for CTV measurement. Indicative of the inherent difficulty identifying tunnel boundaries directly from MRI, the relative changes in volume from neutral were markedly more variable using MRI-based boundary definitions (upwards of 10%) compared to landmarked (<2%) (Table 2). Most notably, both MRI-based landmark strategies showed both increases and decreases in volume relative to the neutral posture, while the anatomically landmarked CTV_3 measure resulted in consistent decreases with both flexion and extension. The posture-related decreases in CTV_3 are compatible with reported increases in carpal tunnel pressure (Gelberman et al., 1981; Keir et al., 1997; Luchetti et al., 1998). The decreased variability observed with anatomically landmarked CTVs is attributable to the combined use of specific bone surface vertices as bony landmarks and inclusion of posture-related changes in the orientation of the tunnel ends. These findings support our choice to use the anatomically landmarked volume as the starting point

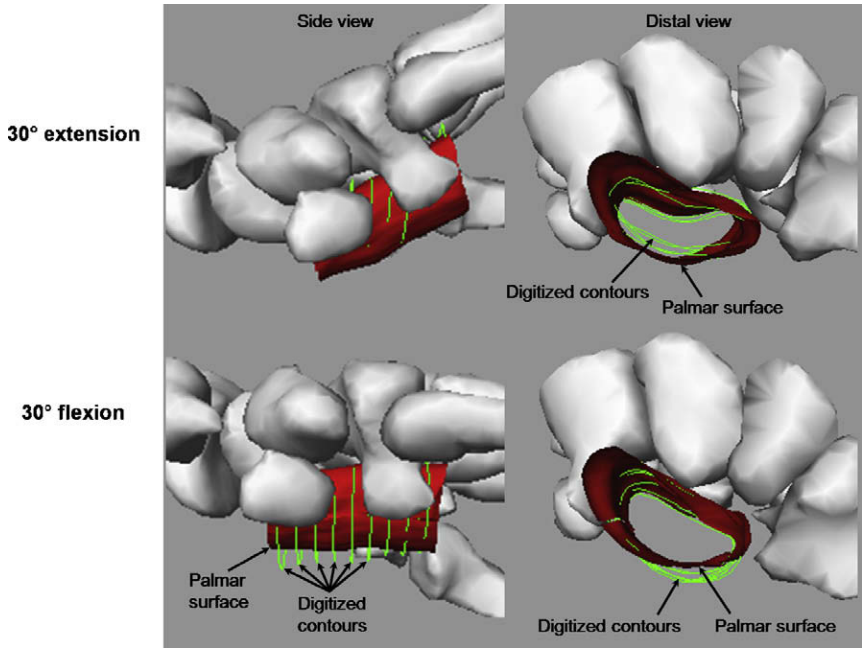

Fig. 3. Comparison of carpal tunnel surfaces with the contours digitized from MRI reveals non-physiological "bellying" of the palmar surface in extension (top, i.e. ligament surface lies palmar to digitized contours), but lack of "bellying" in flexion (bottom, i.e. digitized contours lie palmar to ligament surface).

for the wrist simulations. Unlike previous computer reconstructions which isolated the carpal tunnel (Pierre-Jerome et al., 1997a,b; Mogk and Keir, 2007), the current anatomical landmarking procedure directly linked the carpal tunnel with the carpal bone surfaces, which allowed reliable identification of landmark sites between postures and individuals. Moreover, the current method of combining computerized tunnel reconstructions with modelled bone surfaces is easily adaptable to investigate other boundary definitions used in the literature (Table 3). For example, flexor tendon convergence slightly distal to the capitate-lunate joint and divergence distal to the long finger carpometacarpal joint (Richman et al., 1987, 1989) roughly correspond to the proximal and distal anatomic limits of the flexor retinaculum, respectively (Cobb et al., 1993).

The current evaluation of the carpal tunnel, using modelled bone surfaces to define proximal and distal carpal tunnel boundaries, has made suspected issues with MRI-based boundary identification more apparent. It is typically assumed that the ends of the tunnel are parallel, perhaps by default, due to imaging plane constraints. We have demonstrated the potential effect of this assumption. When all four TCL bony attachment points are used, radial–ulnar asymmetry becomes apparent, with the ulnar aspect of the tunnel longer than the radial in all postures (Fig. 2). Similar proximal-distal asymmetry has been reported using a sagittal tunnel slice in a neutral posture, with the distal aspect of the tunnel showing a greater degree of extension than the proximal end (Keberle et al., 2000). Additionally, tunnel end orientation varies with posture (more so at the distal end), but the orientation of the carpal tunnel is not necessarily a direct reflection of external wrist angle (Mogk and Keir, 2007). These factors likely explain previously reported high inter-subject variability in posture-related volume changes (Bower et al., 2006).

There are several limitations to the current study. First, computerized reconstructions of the carpal tunnel were based on two-dimensional MR images, and would have benefited from the use of three-dimensional imaging methods. Although coarser than desired, the 3 mm slice thickness used was comparable to previous CTV reconstruction studies (ranging from 3 to 5 mm) and offered sufficient slices through each bone to resolve scaling factors and bone positions for each individual. Second, a common set of bone surfaces was used in each wrist-specific model, with each bone scaled uniformly according to wrist size. While this negated individual variation in relative bone size and shape, small differences in landmark locations are unlikely to significantly alter absolute tunnel volume, especially since bone positions were determined on an individual basis for each posture. Finally, the dorsal and palmar tunnel borders were digitized as the inner surfaces of the palmar and transverse carpal ligaments, respectively; thus, the modelled tunnel surfaces effectively "float" amid the carpal bone surfaces. With no physical connection to the bones, the current model assumes that carpal tunnel motion is a function of the weighted average of surrounding bone motions, independent of interaction forces between the ligament and carpal bones.

Inclusion of the bones that surround and anatomically define the carpal tunnel enabled the development of wrist-specific simulations which predicted posture-related carpal tunnel kinematics, and created the framework for future examination of the mechanisms of median nerve trauma. Relating the carpal tunnel to the bones defining it verified concerns regarding the use of MRI-based boundary definitions to estimate carpal tunnel volume, and enabled the evaluation of potential errors. This assessment of volume reconstruction justified the use of landmarked volume in creating each simulation, and revealed consistent posture-related changes in tunnel volume between individuals. When making clinical decisions based on carpal tunnel volumes, it is important that the specific landmarks are noted so that the volume may be compared to those in the literature. Ideally, all appropriate landmarks should be used. The current results indicate that tunnel volume is likely only a partial mechanism for posture-related changes in pressure, and that the soft tissue structures passing through and entering the carpal tunnel are also important elements. While the current investigation concentrated on volume measures, the ability to identify consistent bone surface landmarks may prove valuable in investigating the role of anthropometric parameters in predisposing certain individuals to CTS. Future uses of the model will facilitate the examination of factors that contribute to median

Table 3
Summary of studies evaluating carpal tunnel volume (mm^3), and the image criteria used to define the proximal (***P***) and distal (***D***) carpal tunnel boundaries in extended (E), neutral (N) and flexed (F) wrist postures.

Study	Subject group	# Of subjects	Condition	Volume (mm^3)			Carpal tunnel boundary definitions
				E	N	F	
Current study	Healthy	4M,2F	CTV_1	3922	4332	4286	***P*** – proximal slice through pisiform ***D*** – distal slice through hook of hamate (HH)
			CTV_2	3106	3027	2680	***P*** – proximal slice through pisiform and scaphoid tubercle ***D*** – most distal image with HH and ridge of trapezium (TR)
			CTV_3	3385	3684	3428	***P*** – line bisecting pisiform and scaphoid tubercle ***D*** – line between distal HH to distal TR
Bower et al. (2006)	Healthy	4M,4F	Pinch (0 N)	3475	3737	3722	***P*** – most proximal slice through pisiform ***D*** – most distal slice through hook of hamate
			Corrected[a]	3312		3553	
			Pinch (10N)	3503	3742	3646	
			Corrected[a]	3339		3481	
Pierre-Jerome et al. (1997a)	Asymptomatic	28 F (56 wrists)			10778		***P*** – first slice through radiocarpal joint ***D*** – first slice through bases of metacarpals
	CTS	27 F (36 wrists)			10439		
Pierre-Jerome et al. (1997b)	CTS	28 F (31 wrists)	Pre-op		11512		
			Post-op		13803		
Pierre-Jerome et al. (1997c)	Asymptomatic	30 F	25–45 y.o.		10329		
		27 F	Over 45 y.o.		11086		
Ablove et al. (1994)	Endoscopic release	11 Patients	Pre-op	6100			***P*** – distal edge of the scaphoid ***D*** – appearance of the base of the third metacarpal
			Post-op	7500			
	Subcutaneous release	6 Patients	Pre-op	4600			
			Post-op	5800			
Cobb et al. (1992)	Cadavers	4 (5 wrists)	Imaged		4200		***P*** – distal tip of radial styloid ***D*** – distal aspect of hook of hamate
			Corrected[b]		3430		
Richman et al. (1989)	CTS	6M,6F	Pre-op		6300		***P*** – FCR tendon lying on palmar surface of scaphoid (i.e. outside carpal canal) ***D*** – FPL tendon diverging from other flexor tendons
		15 Wrists	Post-op (6 wk)		7800		
		8 Wrists	Post-op (8 mo)		7500		
Richman et al. (1987)	Cadavers	5 (10 wrists)	Imaged		5840		
			Corrected[b]		4760		

[a] "Corrected" values involved the application of an incremental angle change between the proximal and distal ends for the deviated wrist postures.
[b] "Corrected" values corresponded to volumes determined using silicone molds.

nerve compression, including the relationship between volume and pressure, impingement and force transfer from the flexor tendons.

5. Conflict of interest statement

None declared.

Acknowledgement

This study was supported by an NSERC Discovery grant (#217382-04).

References

Ablove, R.H., Peimer, C.A., Diao, E., Oliverio, R., Kuhn, J.P., 1994. Morphologic changes following endoscopic and two-portal subcutaneous carpal tunnel release. J. Hand Surg. 19A, 821–826.
Armstrong, T.J., Chaffin, D.B., 1979. Carpal tunnel syndrome and selected personal attributes. J. Occup. Med. 21, 481–486.
Bower, J.A., Stanisz, G.J., Keir, P.J., 2006. An MRI evaluation of carpal tunnel dimensions in healthy wrists: implications for carpal tunnel syndrome. Clin. Biomech. 21, 816–825.
Cobb, T.K., Dalley, B.K., Posteraro, R.H., Lewis, R.C., 1992. Establishment of carpal contents/canal ratio by means of magnetic resonance imaging. J. Hand Surg. 17A, 843–849.
Cobb, T.K., Dalley, B.K., Posteraro, R.H., Lewis, R.C., 1993. Anatomy of the flexor retinaculum. J. Hand Surg. 18A, 91–99.
Crisco, J.J., Coburn, J.C., Moore, D.C., Upal, M.A., 2005. Carpal bone size and scaling in men versus in women. J. Hand Surg. 30A, 35–42.
Dekel, S., Papaioannou, T., Rushworth, G., Coates, R., 1980. Idiopathic carpal tunnel syndrome caused by carpal stenosis. Br. Med. J. 280, 1297–1299.
Gelberman, R.H., Hergenroeder, P.T., Hargens, A.R., Lundborg, G.N., Akeson, W.H., 1981. The carpal tunnel syndrome: a study of carpal canal pressures. J. Bone Joint Surg. 63 A, 380–383.
Horch, R.E., Allmann, K.H., Laubenberger, J., Langer, M., Stark, G.B., 1997. Median nerve compression can be detected by magnetic resonance imaging of the carpal tunnel. Neurosurgery 41, 76–82.
Keberle, M., Jenett, M., Kenn, W., Reiners, K., Peter, M., Haerten, R., Hahn, D., 2000. Technical advances in ultrasound and MR imaging of carpal tunnel syndrome. Eur. Radiol. 10, 1043–1050.
Keir, P.J., Wells, R.P., Ranney, D.A., Lavery, W., 1997. The effects of tendon load and posture on carpal tunnel pressure. J. Hand Surg. 22A, 628–634.
Keir, P.J., Bach, J.M., Rempel, D.M., 1998. Effects of finger posture on carpal tunnel pressure during wrist motion. J. Hand Surg. 23 A, 1004–1009.
Ko, C., Brown, T.D., 2007. A fluid-immersed multi-body contact finite element formulation for median nerve stress in the carpal tunnel. Comput. Methods Biomech. Biomed. Eng. 10, 343–349.
Kobayashi, M., Berger, R.A., Nagy, L., Linscheid, R.L., Uchiyama, S., Ritt, M., An, K.N., 1997. Normal kinematics of carpal bones: a three-dimensional analysis of carpal bone motion relative to the radius. J. Biomech. 30, 787–793.
Kung, J., Budoff, J.E., Wei, M.L., Gharbaoui, I., Luo, Z.P., 2005. The origins of the thenar and hypothenar muscles. J. Hand Surg. 30B, 475–476.
Luchetti, R., Schoenhuber, R., Nathan, P., 1998. Correlation of segmental carpal tunnel pressures with changes in hand and wrist positions in patients with carpal tunnel syndrome and controls. J. Hand Surg. 23B, 598–602.

Merhar, G.L., Clark, R.A., Schneider, H.J., Stern, P.J., 1986. High-resolution computer tomography of the wrist in patients with carpal tunnel syndrome. Skeletal Radiol. 15, 549–552.

Mesgarzadeh, M., Schneck, C.D., Bonakdarpour, A., 1989. Carpal tunnel: MR imaging. Part I. Normal anatomy. Radiology 171, 743–748.

Middleton, W.D., Kneeland, J.B., Kellman, G.M., Cates, J.D., Sanger, J.R., Jesmanowicz, A., Froncisz, W., Hyde, J.S., 1987. MR imaging of the carpal tunnel: normal anatomy and preliminary findings in the carpal tunnel syndrome. AJR Am. J. Roentgenol. 148, 307–316.

Mogk, J.P.M., Keir, P.J., 2007. Evaluation of the carpal tunnel based on 3-D reconstruction from MRI. J. Biomech. 40, 2222–2229.

Mogk, J.P.M., Keir, P.J., 2008. Wrist and carpal tunnel size and shape measurements: effects of posture. Clin. Biomech. 23, 1112–1120.

Monagle, K., Dai, G., Chu, A., Burnham, R.S., Snyder, R.E., 1999. Quantitative MR imaging of carpal tunnel syndrome. AJR Am. J. Roentgenol. 172, 1581–1586.

Moojen, T.M., Snel, J.G., Ritt, M.J., Kauer, J.M., Venema, H.W., Bos, K.E., 2002. Three-dimensional carpal kinematics in vivo. Clin. Biomech. 17, 506–514.

Nigro, R.O., 2001. Anatomy of the flexor retinaculum of the wrist and the flexor carpi radialis tunnel. Hand Clin. 17, 61–64.

Pierre-Jerome, C., Bekkelund, S.I., Mellgren, S.I., Nordstrom, R., 1997a. Quantitative MRI and electrophysiology of preoperative carpal tunnel syndrome in a female population. Ergonomics 40, 642–649.

Pierre-Jerome, C., Bekkelund, S.I., Mellgren, S.I., Nordstrom, R., 1997b. Bilateral fast magnetic resonance imaging of the operated carpal tunnel. Scand. J. Plastic Reconstr. Surg. Hand Surg. 31, 171–177.

Pierre-Jerome, C., Bekkelund, S.I., Nordstrom, R., 1997c. Quantitative MRI analysis of anatomic dimensions of the carpal tunnel in women. Surg. Radiol. Anat. 19, 31–34.

Richman, J.A., Gelberman, R.H., Rydevik, B.L., Gylys-Morin, V.M., Hajek, P.C., Sartoris, D.J., 1987. Carpal tunnel volume determination by magnetic resonance imaging three-dimensional reconstruction. J. Hand Surg. 12A, 712–717.

Richman, J.A., Gelberman, R.H., Rydevik, B.L., Hajek, P.C., Braun, R.M., Gylys-Morin, V.M., Berthoty, D., 1989. Carpal tunnel syndrome: morphologic changes after release of the transverse carpal ligament. J. Hand Surg. 14A, 852–857.

Robbins, H., 1963. Anatomical study of the median nerve in the carpal tunnel and etiologies of the carpal-tunnel syndrome. J. Bone Joint Surg. 45A, 953–966.

Rojviroj, S., Sirirchativapee, W., Kowsuwon, W., Wongwiwattananon, J., Tamnanthong, N., Jeeravipoolvarn, P., 1990. Pressures in the carpal tunnel. A comparison between patients with carpal tunnel syndrome and normal subjects. J. Bone Joint Surg. 72B, 516–518.

Silverstein, B.A., Fine, L.J., Armstrong, T.J., 1987. Occupational factors and carpal tunnel syndrome. Am. J. Ind. Med. 11, 343–358.

Skie, M., Zeiss, J., Ebraheim, N.A., Jackson, W.T., 1990. Carpal tunnel changes and median nerve compression during wrist flexion and extension seen by magnetic resonance imaging. J. Hand Surg. 15A, 934–939.

Smith, E.M., Sonstegard, D.A., Anderson, W.H., 1977. Carpal tunnel syndrome: contribution of flexor tendons. Arch. Phys. Med. Rehab. 58, 379–385.

Sora, M.C., Genser-Strobl, B., 2005. The sectional anatomy of the carpal tunnel and its related neurovascular structures studied by using plastination. Eur. J. Neurol. 12, 380–384.

Uchiyama, S., Itsubo, T., Yasutomi, T., Nakagawa, H., Kamimura, M., Kato, H., 2005. Quantitative MRI of the wrist and nerve conduction studies in patients with idiopathic carpal tunnel syndrome. J. Neurol. Neurosurg. Psychiatry 76, 1103–1108.

Weiss, N.D., Gordon, L., Bloom, T., So, Y., Rempel, D.M., 1995. Position of the wrist associated with lowest carpal-tunnel pressure: implications for splint design. J. Bone Joint Surg. 77A, 1695–1699.

Werner, F.W., Short, W.H., Green, J.K., 2005. Changes in patterns of scaphoid and lunate motion during functional arcs of wrist motion induced by ligament division. J. Hand Surg. 30A, 1156–1160.

Yoshioka, S., Okuda, Y., Tamai, K., Hirasawa, Y., Koda, Y., 1993. Changes in carpal tunnel shape during wrist joint motion. MRI evaluation of normal volunteers. J. Hand Surg. 18B, 620–623.